The Non-coherent Squaring Detector and its Application to Bi-phased Signals

Daniele Borio[1], *Member, IEEE*

Abstract

The Non-coherent Squaring Detector (NSD) has been recently derived from the Generalized Likelihood Ratio Test (GLRT) as the linear combination of the non-coherent and squaring detectors. The statistical properties of the NSD are investigated and a simple criterion for fixing the decision threshold is provided. In particular, approximations for the false alarm and detection probabilities are derived and used to characterize the performance of the NSD. The application of the NSD to the detection of pulsed bi-phased signals is then considered. The validity of the theoretical findings is supported by real data analysis and Monte Carlo simulations.

Index Terms

Bit Transition, Detection, False Alarm, Generalized Likelihood Ratio Test, GLRT, bi-phased signals

I. Introduction

Emerging technologies, such as Cognitive Radio (CR) and high-sensitivity Global Navigation Satellite System (GNSS) signal processing, rely on the ability to detect weak signals with power levels below the thermal noise. In CR applications, reliable signal detection is required for revealing the availability of white spaces [3], i.e. allocated frequency bands locally unused. In high-sensitivity GNSS receivers [11], long integration times are required for extracting weak satellite signals from thermal noise. These technologies are two examples where the design of reliable signal detection techniques is of paramount importance. Several strategies have been

1) Institute for the Protection and Security of Citizen (IPSC), Joint Research Centre, Ispra (VA), Italy. Email: daniele.borio@ieee.org

designed to improve the detection capabilities of different systems. In [3], an overview of different detection strategies developed for CR applications is presented. In general, performance is improved by introducing new information regarding the signal to be detected. Specific signal features, such as cyclo-stationarity, can be exploited to make the detection process more reliable. In the specific case of high-sensitivity GNSS receivers, signal detection is primarily based on the coherent detector, i.e. the matched filter. The incoming signal is correlated with a local replica of itself and integrated over a period of time, T_c. Signal samples are coherently accumulated and the noise variance is relatively reduced by a factor proportional to T_c. The integration time is however limited by Doppler frequency uncertainties and data transitions. Thus, post-coherent combining techniques have been introduced to reduce the noise impact even in the presence of the aforementioned impairments. In [20] and [8], robust techniques for the acquisition of GNSS signals affected by Doppler frequencies uncertainties have been developed whereas [16] and [6] considered the problem of signal detection in the presence of data bits.

From the analysis, it emerged that acquisition strategies robust to frequency uncertainties and data transitions are the linear combinations of different detectors. Each detector provides additional information for determining the signal presence. For example, the generalized and averaged post-detection integration schemes derived in [8] are the linear combination of the classical non-coherent detector and several differential integration blocks.

The Non-coherent Squaring Detector (NSD) has been recently derived from the Generalized Likelihood Ratio Test (GLRT) [16] and is the linear combination of the non-coherent and squaring detectors. Although, [16] demonstrated the use of the NSD for the acquisition of weak Global Positioning System (GPS) signal, the algorithm is general and can be easily adopted for the processing of other GNSS signals fully exploiting the benefits of multi-constellation GNSS receivers [2]. Moreover, the application of this detector is not limited to GNSS and the NSD can be used for the detection of any bi-phased signal.

In this paper, the NSD is at first reviewed and its statistical properties are investigated. Although the joint use of several integration schemes improves the overall detection capabilities, it also makes the statistical characterization of the system analytically untreatable. This is often due to the statistical dependence among the different blocks constituting the final detection system. For this reason, closed form expressions for the false alarm and detection probabilities are often unavailable. False alarm refers to the event of erroneously declaring the signal presence whereas

detection occurs when the signal presence is correctly revealed [10]. For the generalized and averaged integration schemes only approximate results based on the fitting of Monte Carlo simulations are available [8]. For the NSD, only Monte Carlo simulation results have been provided by [16] and [6].

The availability of a simple expression for the false alarm probability is particularly important since it is the basis for setting the decision threshold and obtaining a Constant False Alarm Rate (CFAR) detector [10]. In this paper, results relative to the sum of squared complex Gaussian random variables [18], [19] are used to determine the mean and variance of the NSD decision variable and provide approximations for the false alarm and detection probabilities. The false alarm approximation is based on the use of a non-linear transformation for accelerating the rate of convergence of the distribution of the NSD decision variable to that of a Gaussian random variable. In [22], it is shown that the fractional power of a sequence of chi-squared random variables converges in distribution to a Gaussian random variable. The convergence rate is improved by selecting the fractional power which minimizes the skewness of the transformed random variable. This approach is generalized and adopted for deriving a Gaussian approximation of the false alarm probability of the NSD decision variable. In particular, Monte Carlo simulations are used to compute the skewness of the transformed random variable and an iterative procedure is proposed to determine the fractional power. Although Monte Carlo simulations are used, the approximation obtained constitutes a simple criterion for fixing the decision threshold which significantly simplifies the analysis of the NSD decision statistics. The Gaussian approximation derived is valid for a large set of parameters and effectively describes the behavior of the NSD decision variable also in the tail region of its distribution. Note that the proposed approach is general and can be used for other problems involving data fitting.

A simple approximation for the detection probability is also provided and compared with simulation results. Monte Carlo simulations demonstrate the effectiveness of the NSD for the processing of bi-phased signals and its superiority with respect to the standard non-coherent detector.

The application of the NSD to the detection of pulsed bi-phased signals is then discussed. In particular, the problem of detecting pulsed pseudolite signals [5] is considered. The NSD is used to determine the presence of pulsed pseudolite signals and implement pulse blanking. Sample results obtained processing real data are provided and demonstrate the feasibility of the system proposed.

The remainder of this paper is organized as follows. The NSD is briefly introduced in Section II and an alternative formulation of the decision statistic is also provided. A statistical characterization of NSD decision variable is provided in Section III where approximations for the false alarm and detection probabilities are provided. Simulation results are used to support the theoretical findings in Section IV whereas the case of pulsed pseudolite signals is considered in Section V. Finally some conclusions are drawn in Section VI.

II. The Non-coherent Squaring Detector

Consider a set of L complex random variables defined as follows:

$$y_k = Ad_k \exp\{j\varphi\} + \eta_k \tag{1}$$

where A is the signal amplitude and $\{d_k\}_{k=0}^{L-1}$ is a set of independent random variables assuming values in $\{-1, 1\}$ with equal probability. The sequence $\{d_k\}_{k=0}^{L-1}$ can be used, for example, to model the bit sequence transmitted using a digital signal. φ is a uniform random variable assuming values in the interval $(-\pi, \pi]$ and $\{\eta_k\}_{k=0}^{L-1}$ is a set of independent identically distributed (i.i.d.) circularly symmetric complex Gaussian random variables:

$$\eta_k \sim \mathcal{N}_c\left(0, \mathrm{I}_2\sigma^2\right) \tag{2}$$

where σ^2 is the variance of the real and imaginary parts of η_k and I_2 is the 2×2 identity matrix used to denote the lack of correlation between the real and imaginary part of η_k.

The goal of the NSD is to discriminate between the two hypotheses:

- H_0 (null hypothesis): $A = 0$, the signal is absent,
- H_1 (alternative hypothesis): $A \neq 0$, the signal is present.

The NSD was derived in [16] using the GLRT approach. The decision between the two hypotheses is performed by using the input samples, y_k, and computing a decision variable that is compared with a decision threshold. If the threshold is passed, H_1 is selected and the signal is declared present. Otherwise, the signal is declared absent. The NSD decision variable is given by [16]

$$D = \sum_{k=0}^{L-1} |y_k|^2 + \left| \sum_{k=0}^{L-1} y_k^2 \right| \tag{3}$$

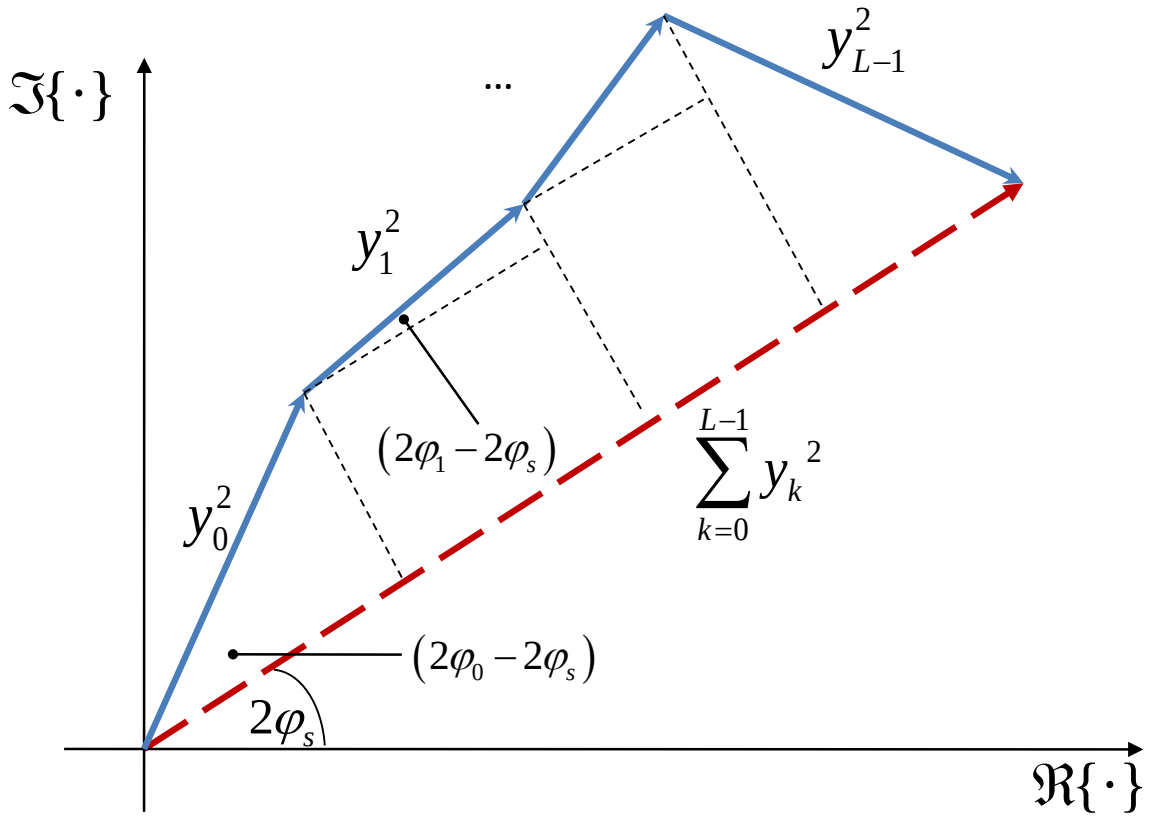

Fig. 1. Geometrical interpretation of the NSD.

that is the sum of two terms. The first one is obtained by non-coherently combining the complex samples (1). This is the classical non-coherent detector used, for example, for CR applications [3]. The second term is the modulus of the sum of the squared samples, y_k, and is thus named squaring detector. The NSD is inherently immune to data bit transitions since both terms in (3) have been obtained through squaring. A geometrical interpretation of the NSD is provided in Fig. 1. The squared samples are interpreted as vectors in the complex plane and the decision variable, D, is the perimeter of the polygon defined by the squared samples and their sum, $S = \sum_{k=0}^{L-1} y_k^2$. Using the geometric interpretation provided in Fig. 1, the following property is

easily found:

$$\begin{aligned} D &= \sum_{k=0}^{L-1} |y_k|^2 \left[1 + \cos\left(2\varphi_k - 2\varphi_s\right)\right] \\ &= 2\sum_{k=0}^{L-1} |y_k|^2 \cos^2\left(\varphi_k - \varphi_s\right) = 2\sum_{k=0}^{L-1} \Re^2\left\{y_k \exp\left\{-j\varphi_s\right\}\right\} \end{aligned} \tag{4}$$

where $\varphi_k = \angle y_k$ and

$$\varphi_s = \frac{1}{2}\angle S = \frac{1}{2}\angle \sum_{k=0}^{L-1} y_k^2. \tag{5}$$

It is noted that the multiplication by $\exp\left\{-j\varphi_s\right\}$ introduces statistical dependence between the different terms in the summations in (4). Formulation (4) allows one to derive bounds on D. For instance, it can be easily shown that $D < 2\sum_{k=0}^{L-1} |y_k|^2$.

The decision variable, D, is used to discriminate the null hypothesis, H_0, of signal absence from the alternative hypothesis, H_1, of signal presence. More specifically, the signal is declared present if $D > T_h$. T_h is the decision threshold which is determined by fixing the probability of false alarm, i.e., the probability of erroneously detecting the signal presence:

$$P_{fa}(T_h) = P(D > T_h | H_0). \tag{6}$$

The detection probability, i.e., the probability of correctly detecting the signal presence is defined as:

$$P_d(T_h) = P(D > T_h | H_1). \tag{7}$$

In the next section, the false alarm and detection probabilities are analyzed and approximate expressions for (6) and (7) are provided.

III. False Alarm and Detection Probabilities

In this section, the statistical properties of (3) are investigated and a simple criterion for fixing the decision threshold is suggested. For the analysis, it is assumed that the variance σ^2 is known. This is the case of GNSS receivers which are equipped with a noise floor estimator [21] which continuously provides estimates of σ^2.

Finding the exact distribution of D is not a simple problem for $L > 1$. This is due to the statistical dependence between the non-coherent and squaring terms present in (3). In the following, the approach adopted in [22] is generalized and used for the characterization of the NSD decision

variable. In [22], a non-linear transformation is used to improve the convergence speed of the probability density function (pdf) of a chi-squared random variable to a Gaussian distribution. In particular, it is shown that if χ^2 is a central chi-squared random variable with F degrees of freedom, then $(\chi^2)^\alpha$ converges to a Gaussian random variable for large F. In [22], $\alpha = \frac{1}{3}$ was selected to improve the convergence speed of the skewness of the transformed random variable, $(\chi^2)^\alpha$, to zero. The use of a Gaussian approximation for $(\chi^2)^\alpha$ is justified on the basis of the saddle-point approximation argument [15].

A similar approach is used here: the decision variable D is at first transformed

$$T = D^\alpha \tag{8}$$

and its pdf is approximated by that of a Gaussian random variable. Finally, the following approximation is obtained

$$P(D > T_h) = P(D^\alpha > T_h^\alpha) \approx \frac{1}{2}\text{erfc}\left(\frac{T_h^\alpha - \mu_T}{\sqrt{2\sigma_T^2}}\right) \tag{9}$$

where μ_T and σ_T^2 are the mean and variance of the transformed random variable. Note that the approach proposed is general and can be used for determining both false alarm and detection probabilities. For this reason, the hypothesis (either H_0 or H_1) is not explicitly specified in (9). Approximation (9) requires the determination of μ_T, σ_T^2 and α. In the following, expressions for μ_T and σ_T^2 are provided whereas α is obtained using an optimization approach based on Monte Carlo simulations.

The mean and variance of (8) can be obtained using the following Taylor series expansion

$$T^n = \mu_D^{n\alpha}\left(1 + \frac{D-\mu_D}{\mu_D}\right)^{n\alpha} \approx \mu_D^{n\alpha}\left[1 + n\alpha\frac{D-\mu_D}{\mu_D} + \frac{n}{2}\alpha(n\alpha-1)\frac{(D-\mu_D)^2}{\mu_D^2}\right] \tag{10}$$

where $\mu_D = \text{E}[D]$ is the mean of the decision variable. The series expansion has been truncated to the second order. The validity of the truncation was verified through Monte Carlo simulations. Setting $n = 1, 2$ and applying the expectation operation on both sides of (10) lead to approximate expressions for the first two moments of T:

$$\mu_T = \text{E}\left[T\right] \approx \mu_D^\alpha\left[1 + \frac{1}{2}\alpha(\alpha-1)\frac{\sigma_D^2}{\mu_D^2}\right] \tag{11}$$

$$\text{E}\left[T^2\right] \approx \mu_D^{2\alpha}\left[1 + \alpha(2\alpha-1)\frac{\sigma_D^2}{\mu_D^2}\right] \tag{12}$$

where σ_D^2 is the variance of D. σ_T^2 is finally computed combining (11) and (12):

$$\sigma_T^2 = \text{Var}\{T\} \approx \alpha^2 \frac{\sigma_D^2}{\mu_D^{2(1-\alpha)}}. \tag{13}$$

The first moment of D under H_1 can be computed using the properties of non-central chi-squared random variables and the results obtained in [18], [19]. In particular, $\mu_D|H_1$ can be expressed as:

$$\mu_D|H_1 = E[D|H_1] = (2L+\lambda)\sigma^2 + \int_0^{+\infty} r f_R(r, L, \lambda) dr \tag{14}$$

where λ is the non-centrality parameter

$$\lambda = L\frac{A^2}{\sigma^2} \tag{15}$$

and $f_R(r, L, \lambda)$ is the pdf of the modulus of the sum of L squared complex Gaussian random variables [18], [19] with non-centrality parameter λ. $f_R(r, L, \lambda)$ can be expressed as [18], [19]

$$f_R(r, L, \lambda) = \frac{r}{4\sigma^4} \int_0^{+\infty} f_L(u, \lambda) J_0\left(\frac{u\lambda}{2(1+u^2)}\right) J_0\left(\frac{ru}{2\sigma^2}\right) du \tag{16}$$

where

$$f_L(u, \lambda) = \frac{u}{(1+u^2)^{L/2}} \exp\left\{-\frac{\lambda}{2}\frac{u^2}{1+u^2}\right\} \tag{17}$$

and $J_0(\cdot)$ is the Bessel function of first kind and zero order [1]. Although (14) requires the use of numerical integrations, an effective approximation can be obtained by exploiting (4). In particular, for sufficiently large λ it is possible to assume

$$\varphi_s \approx \varphi \tag{18}$$

where φ_s has been defined in (5) and φ is the phase of the input samples, y_k. Using (18) and (4), $D|H_1$ can be approximated as

$$\begin{aligned} D &= 2\sum_{k=0}^{L-1} \Re^2\{y_k \exp\{-j\varphi_s\}\} \approx 2\sum_{k=0}^{L-1} \Re^2\{Ad_k + \eta_k \exp\{-j\varphi\}\} \\ &= 2\sum_{k=0}^{L-1} \left(A^2 + 2Ad_k\bar{\eta}_k + \bar{\eta}_k^2\right) \end{aligned} \tag{19}$$

where

$$\bar{\eta_k} = \Re\{\eta_k \exp\{-j\varphi\}\}. \tag{20}$$

It is noted that $\bar{\eta_k}$ are a set of i.i.d. Gaussian random variables with zero mean and variance σ^2. A simple approximation for $\mu_D|H_1$ is finally obtained from (19):

$$\mu_D|H_1 = E\left[D|H_1\right] \approx 2L(A^2+\sigma^2) = 2\sigma^2(\lambda+L). \tag{21}$$

Under H_0, (14) can be significantly simplified and the following expression for $\mu_D|H_0$ is obtained in Appendix I:

$$\mu_D|H_0 = E\left[D|H_0\right] = 2L\sigma^2 + 2\sqrt{\pi}\sigma^2\frac{\Gamma\left(\frac{L+1}{2}\right)}{\Gamma\left(\frac{L}{2}\right)} \tag{22}$$

where $\Gamma(\cdot)$ is the Gamma function [1].

The evaluation of the second moment is more complex and requires the repeated use of numerical integration. Under H_1, a 5-dimensional integral has to be solved and the complexity of the derivation of $E\left[D^2|H_1\right]$ does not provide any additional insight on the properties of $D|H_1$. For this reason, exact expressions are provided only for the H_0 case. Under H_1, it is however possible to derive simple and effective approximations for $E\left[D^2|H_1\right]$ and $\text{Var}\left\{D|H_1\right\}$ using (19). In particular, the following expressions can be easily proved:

$$E\left[D^2|H_1\right] \approx 4L^2(A^2+\sigma^2)^2 + 8L\sigma^2(2A^2+\sigma^2) = 4\sigma^4[(\lambda+L)^2+4\lambda+2L] \tag{23}$$

$$\text{Var}\left\{D|H_1\right\} \approx 8L\sigma^2(2A^2+\sigma^2) = 8\sigma^4(2\lambda+L). \tag{24}$$

The H_0 case is considered in Appendix I where it is shown that

$$\begin{aligned} E\left[D^2|H_0\right] &= 4L(L+1)\sigma^4 + 8L\sigma^4 \\ &+ \frac{4}{\pi}L\int_0^{\infty}\int_0^{+\infty} h(r+h)\text{E}_c\left(\frac{4rh}{(r+h)^2}\right)\cdot f_R(r,L-1)\frac{1}{2\sigma^2}\exp\left\{-\frac{h}{2\sigma^2}\right\}drdh \end{aligned} \tag{25}$$

where $\text{E}_c(\cdot)$ is the complete elliptic integral of second kind [1]. The function

$$f_R(r,L) = f_R(r,L,0)$$

is the pdf of the modulus of the sum of L squared zero mean complex Gaussian random variables. In [18], it is shown that $f_R(r,L)$ can be expressed as

$$f_R(r,L) = \frac{1}{2^{\frac{L}{2}}\sigma^2\Gamma\left(\frac{L}{2}\right)}\left(\frac{r}{2\sigma^2}\right)^{\frac{L}{2}}\text{K}_{\frac{L-2}{2}}\left(\frac{r}{2\sigma^2}\right). \tag{26}$$

where $\text{K}_\nu(\cdot)$ is the modified Bessel function of second kind and order ν [1]. Although (25) requires a double integration, the integrand is a smooth function which quickly converges to

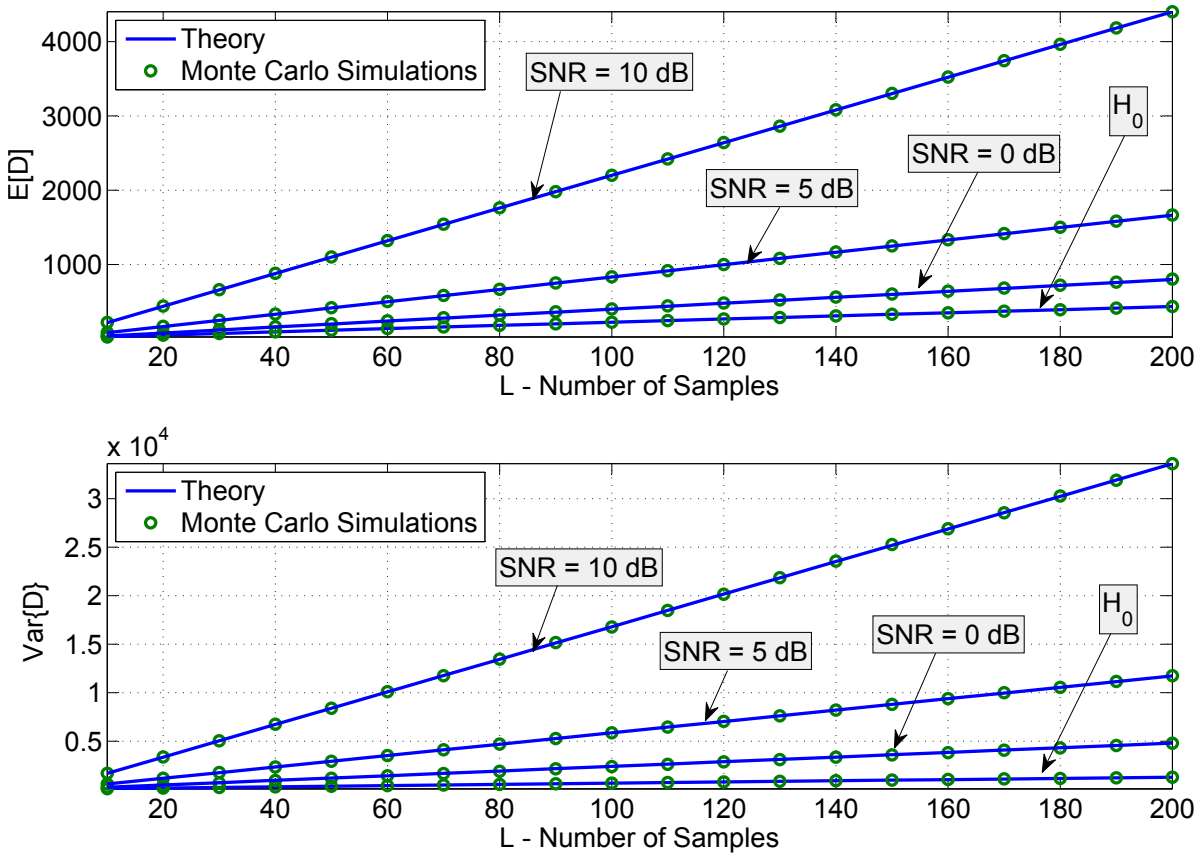

Fig. 2. Mean and variance of the decision variable, D, under the null and alternative hypotheses. Theoretical formulas have been verified through Monte Carlo simulations. 10^7 samples have been used for the Monte Carlo evaluation of mean and variance.

zero. The variance of D can be easily evaluated under H_0 using the results relative to the first two moments. The mean and variance of the decision variable, D, are considered in Fig. 2 where theoretical formulas are compared with Monte Carlo simulations. In Fig. 2, both the H_0 and H_1 cases are considered. Results under H_1 are provided as a function of the Signal-to-Noise Ratio (SNR) defined as

$$SNR = \frac{A^2}{\sigma^2} = \frac{1}{L}\lambda \tag{27}$$

that is the ratio between the useful signal power and the noise variance.

From Fig. 2, a good agreement between theoretical findings and Monte Carlo simulations clearly emerges. For the H_1 case, formulas (21) and (24) have been used showing the effectiveness of approximation (19). Under H_0, μ_D and σ_D^2 increase almost linearly with the number of samples, L, used for the computation of the decision variable. Using formula 6.1.46 of [1], (22) can be

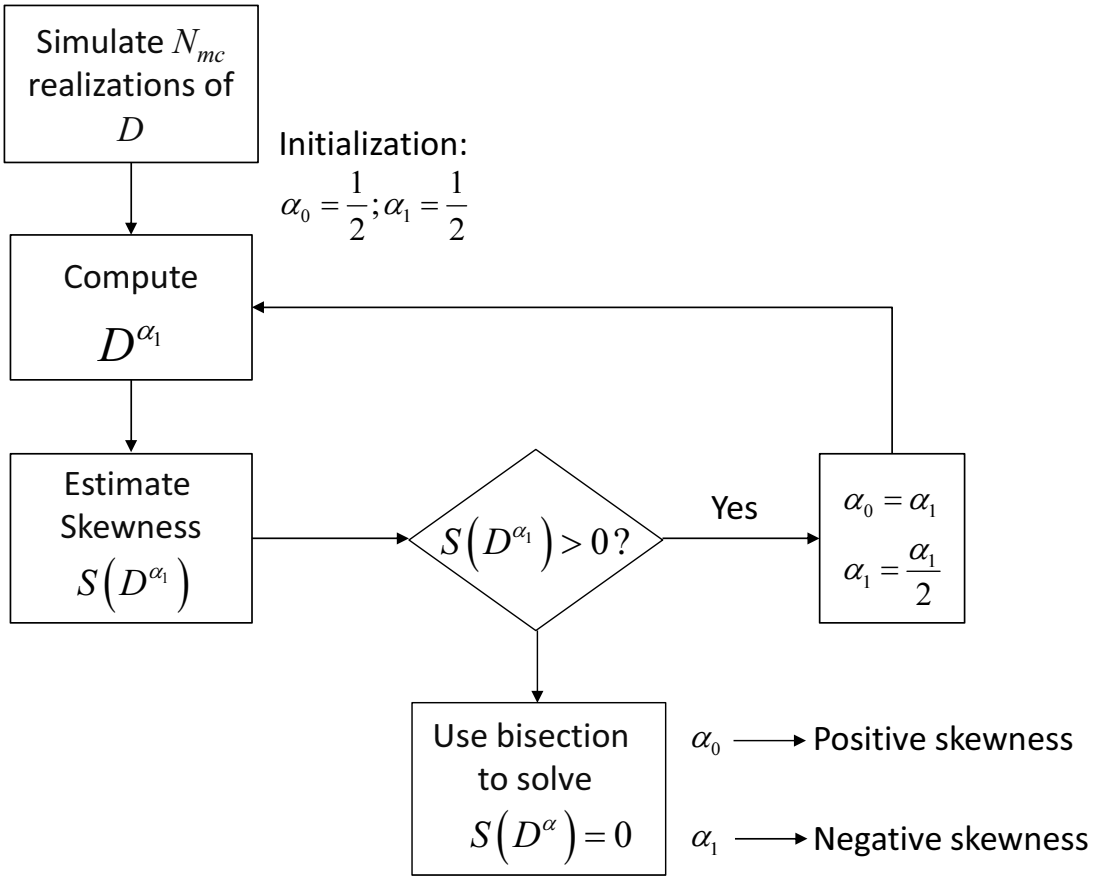

Fig. 3. Procedure adopted for the computation of α, the fractional power used to transform the decision variable and improve the Gaussian approximation. A bisection method is used to minimize the skewness of the transformed decision variable and find α. $N_{mc} = 10^7$ samples are used to estimate the skewness using Monte Carlo simulations.

approximated as

$$\mu_D \approx 2L\sigma^2 + \sqrt{2\pi L}\sigma^2 \tag{28}$$

confirming that for large L, μ_D increases almost linearly. Although $\sigma_D^2|H_0$ does not admit a simple approximation due to the integral form of (25), the values depicted in Fig. 2 can be easily interpolated and σ_D^2 can be approximated by a first order polynomial in L.

The approach used to determine the fractional power, α, in (8) is shown in Fig. 3. In particular, α is selected in order to nullify the skewness of the transformed random variable. Since it was not

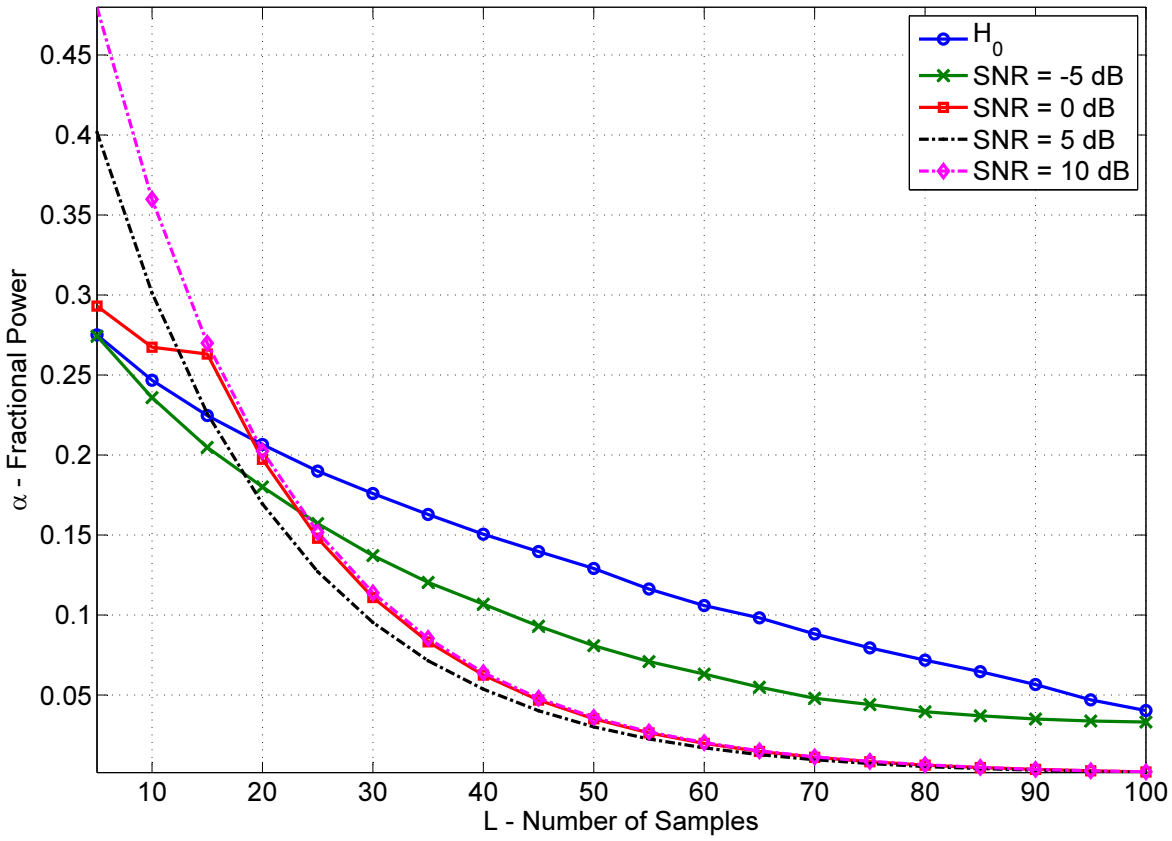

Fig. 4. Fractional power values, α, which nullify the skewness of the transformed decision variable, T, as a function of L, the number of samples used for computing the decision statistic. The values obtained are exponentially decreasing with L.

possible to find a manageable expression for the skewness of T [1] , a Monte Carlo approach was adopted. At first $N_{mc} = 10^7$ realizations of D are generated and the parameter α is iteratively adjusted in order to find two values, α_0 and α_1, leading to positive and negative skewness, respectively. These two values are then used to initialize a bisection process for solving

$$\text{Skew}[D^{\alpha}] = 0 \tag{29}$$

where Skew$[\cdot]$ denotes skewness.

The values of α obtained using this approach are shown in Fig. 4 as a function of L, the number of samples used for the computation of D and for different SNR values. From Fig. 4, it emerges

[1]The approach based on Taylor series expansion used for (11) and (12) does not provide satisfactory results and higher order terms have to be considered.

that α decreases exponentially for large values of L. When the H_0 case is considered, α can be effectively approximated as

$$\alpha \approx \exp\left\{-0.018L - 1.22\right\}. \tag{30}$$

The effectiveness of (30) for determining α even outside the range of values of L considered in Fig. 4 is analyzed using Monte Carlo simulations in Section IV.

Using (11), (12) and (30) it is finally possible to compute the Gaussian approximation of the NSD false alarm probability and the decision threshold can be set as

$$T_h = \left[\sqrt{2\sigma_T^2}\text{erfc}^{-1}\left(2P_{fa}^t\right) + \mu_T\right]^{\frac{1}{\alpha}} \tag{31}$$

where P_{fa}^t is the target false alarm probability.

When the alternative hypothesis is considered, the detection probability can be computed either using the Gaussian approximation discussed above or using (19). When a sufficiently large λ is considered, $D|H_1$ can be approximated as a scaled non-central chi-squared and the probability of detection can be expressed as

$$P_d\left(T_h\right) \approx Q_{L/2}\left(\sqrt{\lambda}, \sqrt{\frac{T_h}{2\sigma^2}}\right) \tag{32}$$

where $Q_l\left(\cdot,\cdot\right)$ is the generalized Marcum Q function of order l [12]. The validity of the two approximations suggested for the detection probability will be further investigated in Section IV using Monte Carlo simulations.

IV. Simulation Results

In this section, the validity of the theoretical approximations derived in Section III is investigated using Monte Carlo simulations.

The false alarm probability of the NSD is provided in Fig. 5 for different values of L, the number of samples used for computing the decision statistic. Curves obtained using Monte Carlo simulations are compared with theoretical approximation (9), where α, μ_T and σ_T^2 have been computed using the approach described in Section III. From Fig. 5, it emerges that approximation (9) is able to effectively capture the statistical behavior of the decision variable, D, under H_0. The approximation proposed is effective also in the tail region of the distribution of $D|H_0$. This clearly emerges from the fact that $P_{fa}(T_h)$ is well approximated by (9) for values as low as 10^{-6}. Note that the curves in Fig. 5 have been obtained using 10^7 simulation runs, thus probability

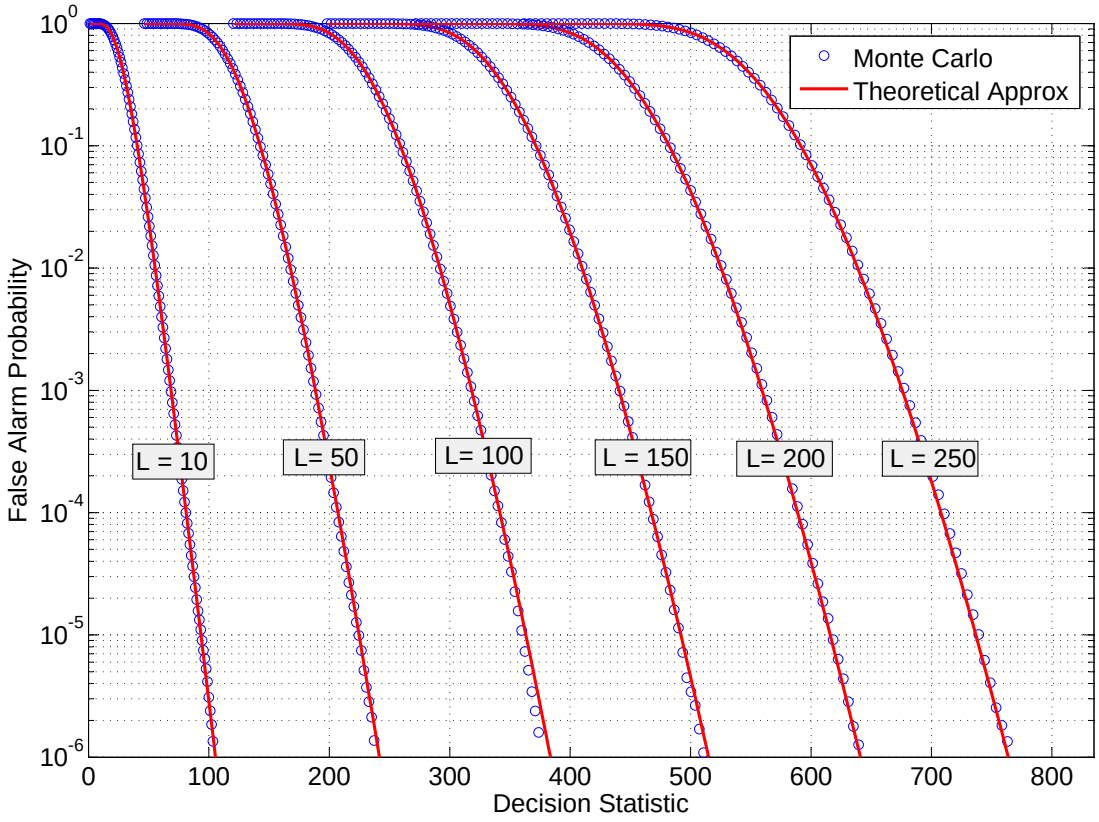

Fig. 5. False alarm probabilities of the NSD: Monte Carlo simulations are compared with approximation (9). $N = 10^7$ realizations were used to estimate the false alarm probability. The input noise variance, σ^2, has been normalized to 1.

values lower than 10^{-6} have not been considered.

In Fig. 5, the behavior of $D|H_0$ has been investigated for values of L up to 250. Although this range is greater than that considered in Fig. 4 for determining (30), the approximation provided for α is effective for all the cases considered. More specifically, the continuous curves in Fig. 5 have been obtained using (30) that provides a valid approximation for the fractional power coefficient. The results shown in Fig. 5 support the validity of the theory developed in Section III and the effectiveness of (5).

The validity of the approximations proposed for the detection probability are investigated in Fig. 6 where two SNR values are considered. For low SNR values, the Gaussian approximation is preferable whereas (32) becomes more effective as λ increases. For $SNR = 5$ dB a good match between Monte Carlo simulations and (32) is found showing the effectiveness of (19) even for moderate SNR values.

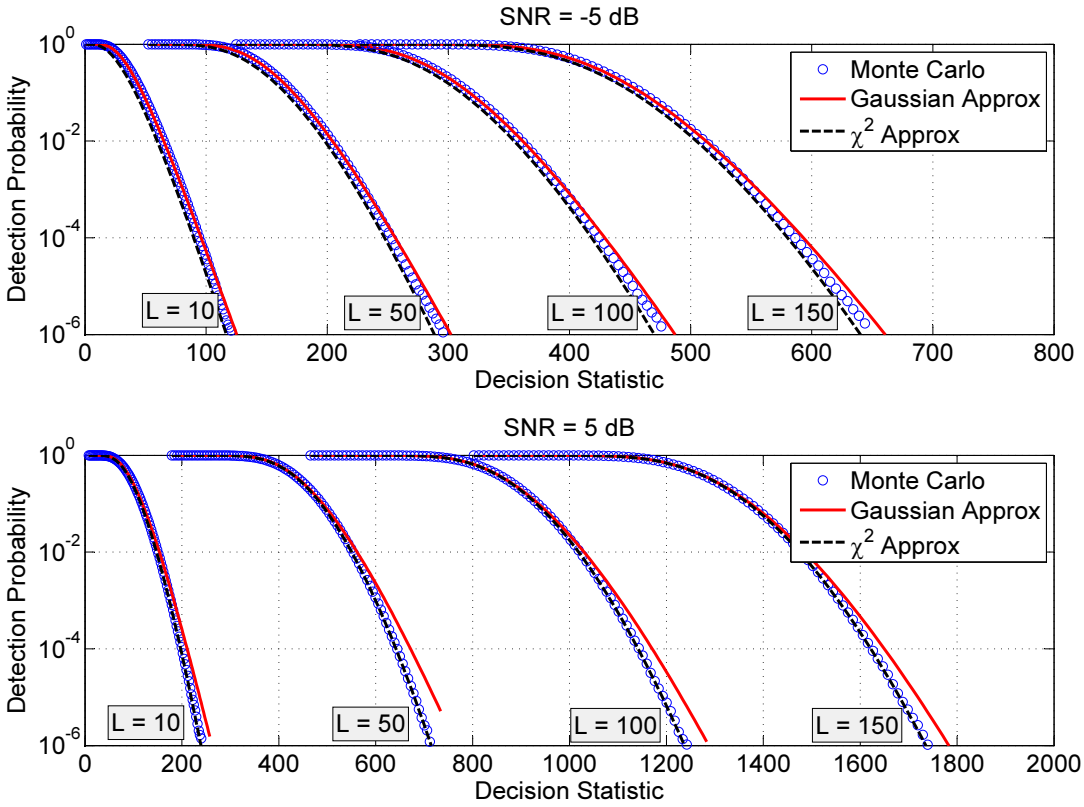

Fig. 6. Detection probability of the NSD: Monte Carlo simulations are compared with approximations (9) and (32). Two different SNR values are considered showing the range of applicability of the proposed approximations. $N = 10^7$ realizations were used to estimate the detection probability. The input noise variance, σ^2, has been normalized to 1.

The detection capability of the NSD are further investigated using Monte Carlo simulations in Fig. 7 where Receiver Operating Characteristics (ROCs) for different values of L are provided. A ROC provides the detection probability as a function of the false alarm rate [10]. A low SNR ($SNR = 0$ dB) is considered and, as expected, the detection capabilities improve with L, the number of samples used for the computation of the decision variable. Performance of the NSD is compared with that of the non-coherent detector [10]. The NSD always outperforms the non-coherent detector showing the advantages of this type of technique. Also in this case, 10^7 simulation runs were used.

Finally, the detection probability of the NSD is provided in Fig. 8 as a function of the input SNR for a fixed false alarm rate, $P_{fa} = 10^{-3}$. As the number of samples, L, increases a lower input SNR is required for achieving the same level of detection probability. Also in this case,

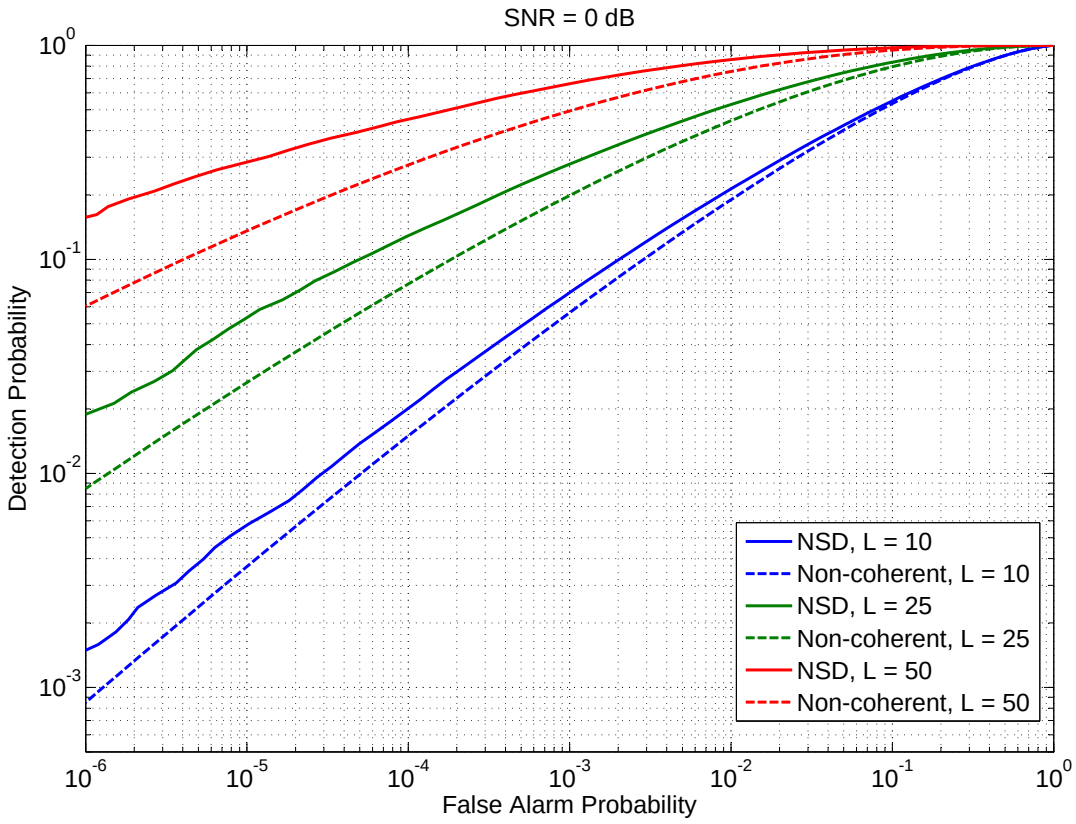

Fig. 7. ROC for the NSD evaluated for $SNR = 0$ dB. The performance of the non-coherent detector is provided as a comparison term.

the performance of the non-coherent detector is provided as a comparison term. The superiority of the NSD emerges clearly.

The results presented in this section confirm the validity of the theoretical characterization provided in Section III and show the superiority of the NSD with respect to standard detection schemes such as the non-coherent detector.

V. Pulsed Pseudolite Signal Detection

The NSD is an effective tool for the detection of bi-phased signals and can be used in different contexts. For instance, [16] demonstrated its use for the detection of weak GNSS signals whereas [5] adopted it for the synchronization of pulsed pseudolite signals. In the following, an additional application of the NSD is suggested. The NSD can be used to detect the presence of pulsed pseudolite signals and implement pulse blanking [9]. A class of pseudolite [7], [17] uses pulsed

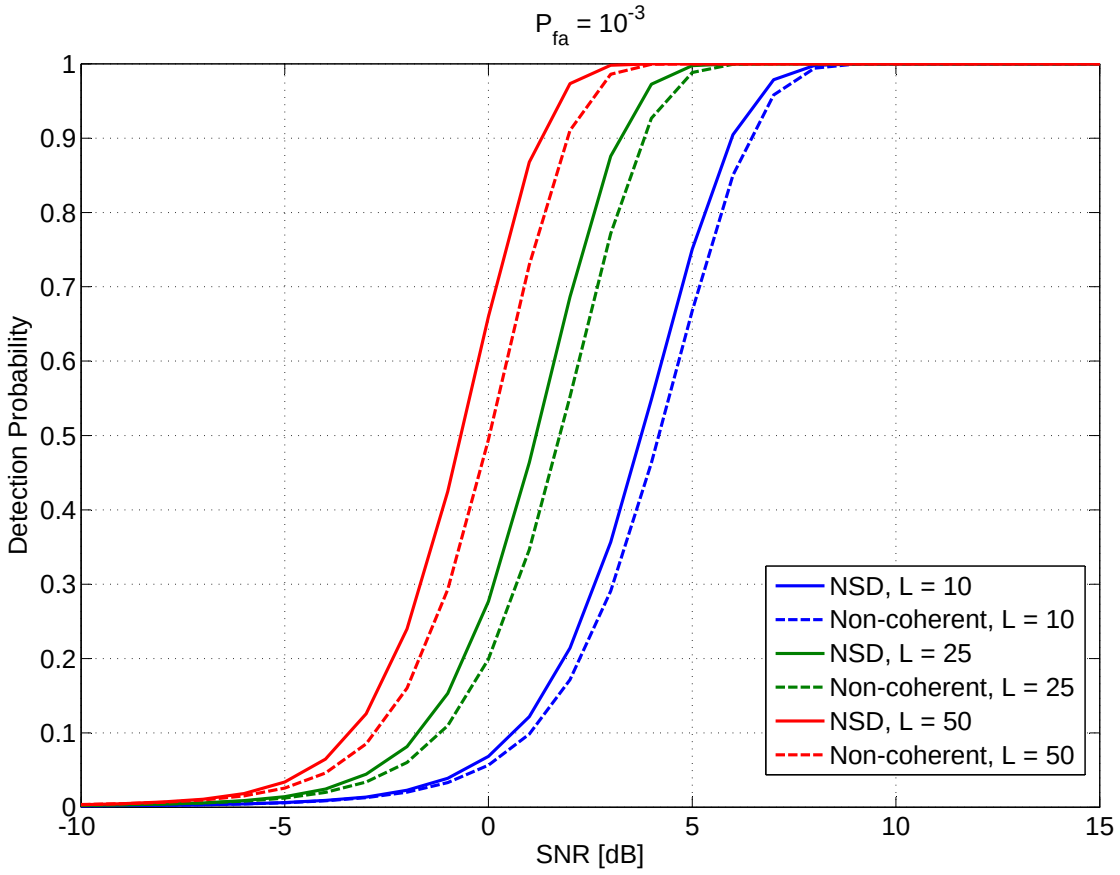

Fig. 8. Detection probability of the NSD as a function of the input SNR for a fixed false alarm rate, $P_{fa} = 10^{-3}$. The performance of the non-coherent detector is provided as comparison term.

signals to reduce interference with other systems such as GNSS. Compatibility can be further improved if pseudolite pulses are detected and excised [14]. For this reason, pulse blanking [9], [14] has been suggested as an effective technique to reduce interference problems. In standard pulse blanking [9], [14] the modulus of the input samples is directly compared against a threshold. If the threshold is passed, the pulse is declared present and pulse excision is performed. This type of processing can be unreliable and can be improved by using the NSD. In particular, pseudolite signals are bi-phased and model (1) is valid. A schematic representation of the pulse blanker implemented using the NSD is shown in Fig. 9. In particular, the input samples, y_k, are used to compute the decision statistic, D. The decision threshold is computed using (31). Note that (31) requires the knowledge of the input noise variance, σ^2, which is estimated using a robust variance estimator [13]. The noise variance is estimated considering short data blocks. Several

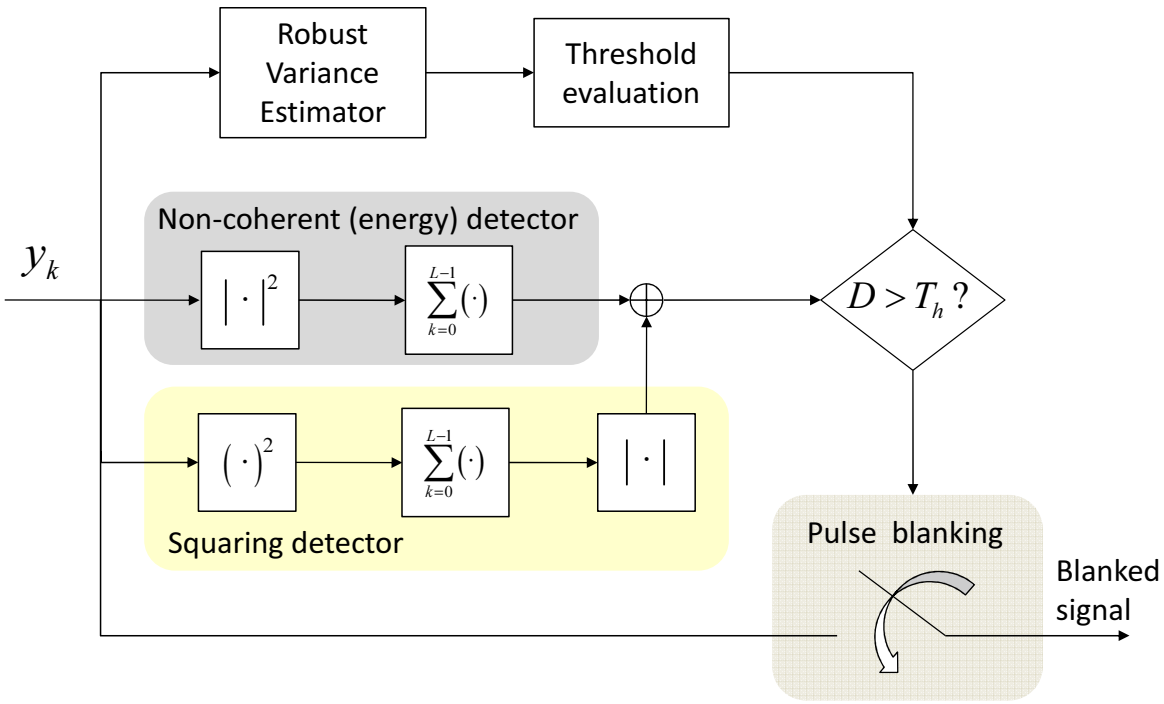

Fig. 9. Implementation of pulse blanking using the NSD. The summations in (3) are implemented using a moving average filter.

estimates (ten for the experiments detailed in the following) are then stored in memory and the final variance is obtained as the median of the stored values:

$$\sigma^2 = \text{MED}\left(\hat{\sigma}_0^2, \hat{\sigma}_1^2, ..., \hat{\sigma}_{P-1}^2\right). \tag{33}$$

In (33), $\{\hat{\sigma}_0^2\}_{i=0}^{P-1}$ are the sample variances computed using subsequent data blocks. The symbol "MED" is used to denote the median operation [13] which is robust against outliers. Since short data blocks are considered, several of them do not contain any signal pulse and provide an unbiased estimates of σ^2. The median operator is used to discard abnormal variance estimates obtained in the presence of interference pulses. The effectiveness of (33) has been empirically verified and its detailed analysis is beyond the scope of this paper.

The variance, σ^2, is used to compute the threshold T_h which is compared against the decision variable, D. If $D > T_h$, then pulse blanking is performed and the samples corrupted by pulsed interference are removed.

Sample results obtained processing pulsed pseudolite signals are shown in Fig. 10. Pulse

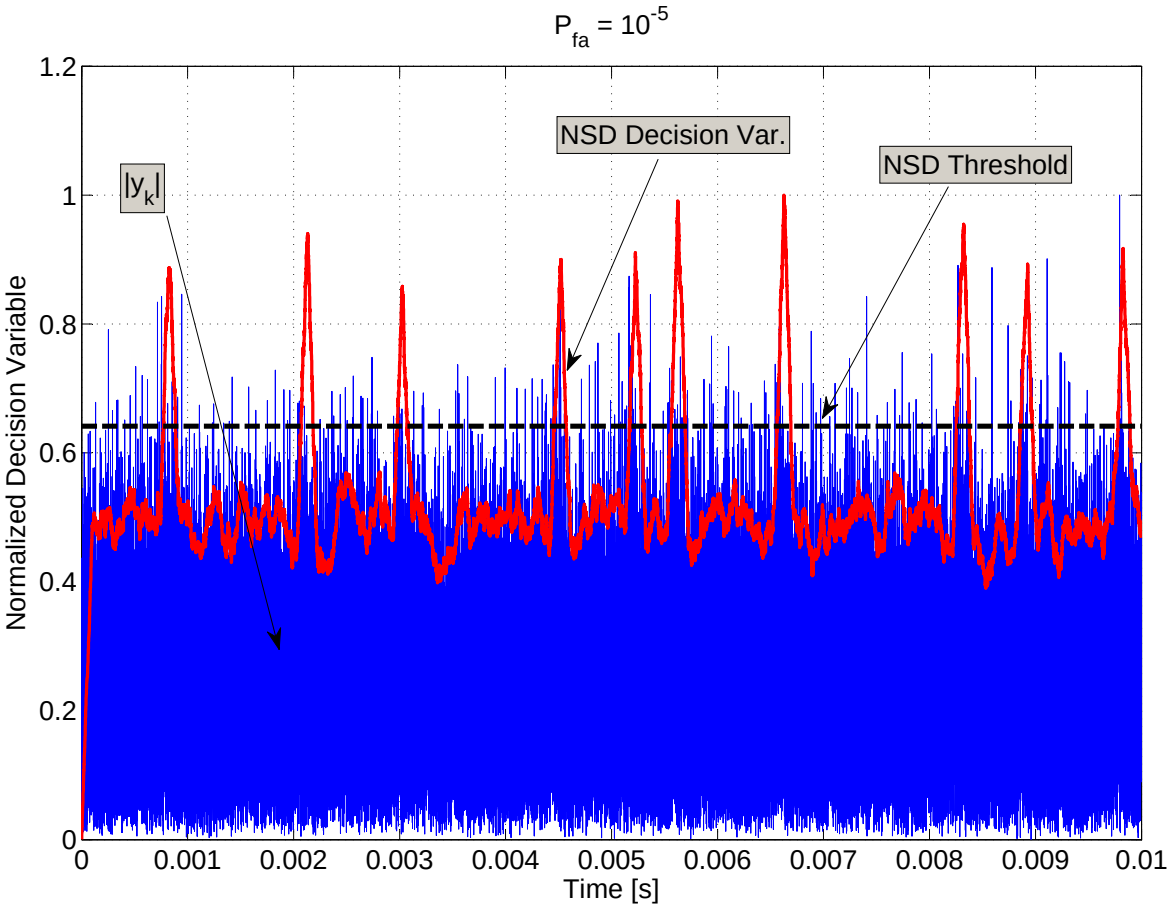

Fig. 10. Sample results obtained processing pulsed pseudolite signals. The NSD is able to detect pulses buried in noise. $SNR = -15$ dB, $L = 500$. The decision statistic has been normalized with respect to the maximum value observed in the dataset.

pseudolite signals were generated using the pseudolite prototype developed in [5] and operating in the GPS L1 band. Raw data samples were collected using a National Instruments (NI) PXI-e5663 Radio Frequency Signal Analyzer (RFSA) with a 14-bit Analog-to-Digital Converter (ADC) and stored on a hard drive for post-processing. The decision variable computed by the NSD is shown in Fig. 10 along with the decision threshold computed for a false alarm probability, $P_{fa} = 10^{-5}$. Although the input signal is characterized by a weak SNR (-15 dB), the NSD is able to correctly detect the pulse presence and enable pulse blanking. In this case, $L = 500$ samples were used for computing the decision variable. The absolute value of the input samples, $|y_k|$, is also shown in Fig. 10: no clear pattern emerges from the noise floor and signal pulses cannot be identified.

The use of the modulus, $|y_k|$, does not allow reliable pulse detection and blanking.

VI. Conclusions

In this paper, the statistical properties of the NSD have been analyzed and the first two moments of the decision variable have been determined and used for deriving approximations for the false alarm and detection probabilities. More specifically, a general approach, based on the use of a non-linear transformation, has been proposed and used to find a Gaussian approximation of the false alarm and detection probabilities. The method proposed is general and can be applied to other data fitting problems. The validity of the methodology proposed has been verified using Monte Carlo simulations: the results obtained constitute a simple criterion for computing the false alarm probability and setting the decision threshold. The detection probability has also been analyzed using an effective approximation determined exploiting a new geometrical interpretation of the NSD decision variable. Monte Carlo simulations support the validity of the theoretical analysis and show the superiority of the NSD with respect to traditional techniques such as the non-coherent detector.

Finally, the use of the NSD for pulsed pseudolite signal detection has been considered and an enhanced pulse blanking scheme has been proposed. The superiority of the suggested approach has also been demonstrated using real pseudolite signals.

Appendix I
First and Second Moments under H_0

In this appendix, the first two moments of the decision statistics (3) are computed under H_0. When the hypothesis is not specified, the result provided is valid under both H_0 and H_1.

The first moment of D can be easily obtained exploiting the linearity of the expected value:

$$E[D] = E\left[\sum_{k=0}^{L-1} |y_k|^2\right] + E\left[\left|\sum_{k=0}^{L-1} y_k^2\right|\right]. \tag{34}$$

Under H_0, the first term in (34) is the mean of a scaled central chi-squared random variable with $2L$ degrees of freedom and is given by

$$E\left[\sum_{k=0}^{L-1} |y_k|^2 \,\middle|\, H_0\right] = 2L\sigma^2. \tag{35}$$

The second term is the mean of the modulus of the sum of squared complex Gaussian random variables [18], [19]. In the following, the notation R_L is used to denote this type of random variable where L indicates the number of terms present in the summation. The mean of R_L has been obtained by [18], [19] and is given by

$$E\left[R_L \middle| H_0\right] = 2\sqrt{\pi}\sigma^2 \frac{\Gamma\left(\frac{L+1}{2}\right)}{\Gamma\left(\frac{L}{2}\right)}. \tag{36}$$

Combining (34) and (36), (22) is obtained. The second moment of D can be obtained as follows:

$$\begin{aligned} E\left[D^2\right] &= E\left[\left(\sum_{k=0}^{L-1}|y_k|^2 + \left|\sum_{k=0}^{L-1} y_k^2\right|\right)^2\right] \\ &= E\left[\left(\sum_{k=0}^{L-1}|y_k|^2\right)^2\right] + E\left[\left|\sum_{k=0}^{L-1} y_k^2\right|^2\right] + 2E\left[\sum_{k=0}^{L-1}|y_k|^2\left|\sum_{i=0}^{L-1} y_i^2\right|\right] \end{aligned} \tag{37}$$

The first term in (37) is the second moment of a scaled central chi-squared random variable and is given by

$$E\left[\left(\sum_{k=0}^{L-1}|y_k|^2\right)^2 \middle| H_0\right] = 4L(L+1)\sigma^4. \tag{38}$$

The second term can be obtained exploiting the results provided by [18], [19] and is given by

$$E\left[\left|\sum_{k=0}^{L-1} y_k^2\right|^2 \middle| H_0\right] = 8L\sigma^4 \tag{39}$$

The evaluation of the cross term in (37) is more complex and requires additional manipulations. More specifically,

$$\begin{aligned} E\left[\sum_{k=0}^{L-1}|y_k|^2\left|\sum_{i=0}^{L-1} y_i^2\right|\right] &= \sum_{k=0}^{L-1} E\left[|y_k|^2\left|\sum_{i=0}^{L-1} y_i^2\right|\right] = LE\left[|y_k|^2\left|\sum_{i=0}^{L-1} y_i^2\right|\right] \\ &= LE_{|y_k|^2}\left[|y_k|^2 E\left[\left|\sum_{i=0,i\neq k}^{L-1} y_i^2 + y_k^2\right| \middle| |y_k|^2\right]\right] \end{aligned} \tag{40}$$

The following notation is introduced to compute $E\left[\left|\sum_{i=0,i\neq k}^{L-1} y_i^2 + y_k^2\right| \middle| |y_k|^2\right]$:

- $S_{L-1} = \sum_{i=0,i\neq k}^{L-1} y_i^2 = R_{L-1}e^{j\varphi_R}$
- $y_k^2 = He^{j\varphi_H}$.

Using this notation, $E\left[\left|\sum_{i=0,i\neq k}^{L-1} y_i^2 + y_k^2\right| \left| |y_k|^2\right.\right]$ can be expressed as

$$\begin{aligned} E\left[\left|\sum_{i=0,i\neq k}^{L-1} y_i^2 + y_k^2\right| \left| |y_k|^2\right.\right] &= E\left[\left|R_{L-1}e^{j\varphi_R} + He^{j\varphi_H}\right| \left| H\right.\right] \\ &= E\left[\sqrt{R_{L-1}^2 + H^2 + 2R_{L-1}H\cos\left(\varphi_R - \varphi_H\right)}\right| H\Bigg]. \end{aligned} \tag{41}$$

Under H_0, φ_R and φ_H are uniformly distributed and using the cosine folding properties [4], $\varphi_R - \varphi_H$ can be replaced by a single random variable, φ, uniformly distributed on $(-\pi, \pi]$. Then

$$\begin{aligned} E\left[\left|\sum_{i=0}^{L-1} y_i^2\right| \left| |y_k|^2\right.\right] &= \frac{1}{2\pi}\int_0^{+\infty} f_R(r, L-1)\int_{-\pi}^{\pi}\sqrt{r^2 + H^2 + 2rH\cos\varphi}d\varphi dr \\ &= \frac{1}{2\pi}\int_0^{+\infty} f_R(r, L-1)\int_{-\pi}^{\pi}\sqrt{r^2 + H^2 + 2rH - (2rH - 2rH\cos\varphi)}d\varphi dr \\ &= \frac{1}{2\pi}\int_0^{+\infty} f_R(r, L-1)\int_{-\pi}^{\pi}\sqrt{(r+H)^2 - 4rH\frac{1-\cos\varphi}{2}}d\varphi dr \\ &= \frac{1}{2\pi}\int_0^{+\infty} f_R(r, L-1)(r+H)\int_{-\pi}^{\pi}\sqrt{1 - \frac{4rH}{(r+H)^2}\sin^2\left(\frac{\varphi}{2}\right)}d\varphi dr \\ &= \frac{1}{2\pi}\int_0^{+\infty} 4f_R(r, L-1)(r+H)\int_0^{\pi/2}\sqrt{1 - \frac{4rH}{(r+H)^2}\sin^2\theta}d\theta dr \\ &= \frac{2}{\pi}\int_0^{+\infty}(r+H)\mathrm{E}_c\left(\frac{4rH}{(r+H)^2}\right) f_R(r, L-1)dr \end{aligned} \tag{42}$$

where $\mathrm{E}_c(\cdot)$ is the complete elliptic integral of second kind [1] and $f_R(r, L-1)$ is defined in (26).

Finally, previous results lead to

$$\begin{aligned} E\left[\sum_{k=0}^{L-1}|y_k|^2\left|\sum_{i=0}^{L-1} y_i^2\right|\right] &= \frac{2}{\pi}L\int_0^{\infty} h\int_0^{+\infty}(r+h)\mathrm{E}_c\left(\frac{4rh}{(r+h)^2}\right) f_R(r, L-1)f_H(h)drdh \\ &= \frac{2}{\pi}L\int_0^{\infty}\int_0^{+\infty} h(r+h)\mathrm{E}_c\left(\frac{4rh}{(r+h)^2}\right) f_R(r, L-1)\frac{1}{2\sigma^2}\exp\left\{-\frac{h}{2\sigma^2}\right\}drdh \end{aligned} \tag{43}$$

where the fact that H is exponentially distributed, i.e.

$$f_H(h) = \frac{1}{2\sigma^2}\exp\left\{-\frac{h}{2\sigma^2}\right\}, \tag{44}$$

has been exploited.

Eq. (25) is obtained combining (38), (39) and (43).

REFERENCES

[1] Abramowitz, M. and Stegun, I. A.: *Handbook of Mathematical Functions with Formulas, Graphs, and Mathematical Tables*. Dover, New York, 1964.

[2] Angrisano, A., Gaglione, S., and Gioia, C.: 'Performance assessment of GPS/GLONASS single point positioning in an urban environment'. *Acta Geodaetica et Geophysica*, pp. 1–13, Jan. 2013.

[3] Axell, E., Leus, G., Larsson, E., and Poor, H.: 'Spectrum sensing for cognitive radio : State-of-the-art and recent advances'. *IEEE Signal Processing Mag.*, vol. 29, no. 3 pp. 101 –116, May 2012. doi:10.1109/MSP.2012.2183771.

[4] Borio, D.: 'GNSS acquisition in the presence of continuous wave interference'. *IEEE Trans. Aerosp. Electron. Syst.*, vol. 46, no. 1 pp. 47 –60, Jan. 2010.

[5] Borio, D., Cano, E., and Baldini, G.: 'Sychronization of pulsed pseudolite signals: Analysis and comparison'. In *Proc. of the ION/GNSS*, pp. 482–493. Nashville, TN, Sep. 2012.

[6] Chandrasekhar, J. and Murthy, C. R.: 'Robust GNSS signal detection in the presence of navigation data bits'. In *Proc, of the IEEE International Conference on Acoustics, Speech and Signal Processing (ICASSP)*, pp. 4344 –4347. May 2011.

[7] Cobb, S. H.: *GPS pseudolites: Theory, Design and Applications*. Phd thesis, Stanford University, Sep. 1997.

[8] Corazza, G. and Pedone, R.: 'Generalized and average likelihood ratio testing for post detection integration'. *IEEE Trans. Commun.*, vol. 55, no. 11 pp. 2159 –2171, Nov. 2007.

[9] Grabowski, J. and Hegarty, C.: 'Characterization of l5 receiver performance using digital pulse blanking'. In *Proc. of the ION GPS*, pp. 1630–1635. Portland, OR, sep 2002.

[10] Kay, S. M.: *Fundamentals of Statistical Signal Processing, Volume 2: Detection Theory*, vol. 2. Prentice Hall, 1st ed., February 1998.

[11] MacGougan, G., Lachapelle, G., Klukas, R., Siu, K., Garin, L., Shewfelt, J., and Cox, G.: 'Performance analysis of a stand-alone high-sensitivity receiver'. *GPS Solutions*, vol. 6, no. 3 pp. 179–195, Dec. 2002.

[12] Marcum, J.: 'A statistical theory of target detection by pulsed radar'. *IRE Transactions on Information Theory*, vol. 6, no. 2 pp. 59–267, Apr. 1960. doi:10.1109/TIT.1960.1057560.

[13] Maronna, R. A., Martin, D. R., and Yohai, V. J.: *Robust Statistics: Theory and Methods*. Series in Probability and Statistics. Wiley, May 2006.

[14] Pany, T.: *Navigation Signal Processing for GNSS Software Receivers*. GNSS Technology and Applications. Artech House, Jan. 2010.

[15] Papoulis, A.: *The Fourier Integral and its Applications*. Mc Graw-Hill, 1978.

[16] Satyanarayana, S., Borio, D., and Lachapelle, G.: 'A non-coherent block processing architecture for standalone GNSS weak signal tracking'. In *Proc. of the ION/GNSS*, pp. 1777–1785. Portland, OR, sep 2011.

[17] Stansell, T. A.: 'RTCM SC-104 recommended pseudolite signal specification'. *NAVIGATION: Journal of The Institute of Navigation*, vol. 33, no. 1 pp. 42–59, Spring 1986.

[18] Tavares, G. and Tavares, L.: 'On the statistics of the sum of squared complex gaussian random variables'. *IEEE Trans. Commun.*, vol. 55, no. 10 pp. 1857 –1862, Oct. 2007. doi:10.1109/TCOMM.2007.906387.

[19] Tavares, G. N. and Tavares, L. M.: 'Statistical characterization of the sum of squared complex gaussian random variables'. Tech. Rep. 3036/2006, Instituto Superior Técnico INESCID, Lisboa, Mar. 2006.

[20] Villanti, M., Salmi, P., and Corazza, G. E.: 'Differential post detection integration techniques for robust code acquisition'. *IEEE Trans. Commun.*, vol. 55, no. 11 pp. 2172 –2184, Nov. 2007.

[21] Ward, P. W.: 'Design technique for precise GNSS receiver post-correlation noise floor measurements with usage design examples by the search and tracking processes'. In *Proc. of ION/ITM*, pp. 607–617. San Diego, CA, Jan. 2010.

[22] Wilson, E. B. and Hilferty, M. M.: 'The distribution of chi-square'. In *Proc. of the National Academy of Sciences*, p. 684688. Washington, Nov. 1931.